

Noise reduction in 3D noncollinear parametric amplifier

Piotr Migdał* and Wojciech Wasilewski

Institute of Experimental Physics, University of Warsaw, Hoża 69, PL-00-681 Warsaw, Poland

We find analytically an approximate Bloch-Messiah reduction of a noncollinear parametric amplifier pumped with a focused monochromatic beam. We consider type I phase matching. The results are obtained using a perturbative expansion and scaled to high gain regime. They allow a straightforward maximization of the signal gain and minimization of the parametric fluorescence noise. We find fundamental mode of the amplifier which is an elliptic Gaussian defining optimal seed beam shape. We conclude that the output of the amplifier should be stripped of higher order modes, which are approximately Hermite-Gaussian beams. Alternatively, the pump waist can be adjusted such that the amount of noise produced in the higher order modes is minimized.

PACS numbers: 42.65.Yj Optical parametric oscillators and amplifiers,
42.65.Re Ultrafast processes; optical pulse generation and pulse compression,
42.65.Lm Parametric down conversion and production of entangled photons.

1. INTRODUCTION

Parametric down-conversion is an important and versatile source of light. Its applications span from amplification of laser pulses to creation of strictly quantum states as entangled photon pairs and the squeezed vacuum. As optical parametric amplifiers rely on nonresonant nonlinear interaction they can be utilized to amplify extremely broadband pulses. One of the most appealing realizations of this phenomenon is the Optical Parametric Chirped Pulse Amplifier (OPCPA) [1, 2] in which the ultrashort pulses are stretched, amplified and then compressed again. The gain medium is typically pumped by a nanosecond second harmonic pulse from a Q-switched laser. Such amplifiers can provide a few femtosecond long multi-terawatt pulses [3, 4].

One of the most important and fundamental problems of this type of amplifiers is the presence of the spontaneous parametric fluorescence which unavoidably accompanies useful gain and compromises pulse contrast ratio. This issue is central in many applications and has been extensively studied [5, 6, 7]. Although the numerical results provided in [7] are very accurate, they are based on Langevin noise equations [8] developed for a cavity parametric amplifier. Consequently, the noise parameter have to rely on an experimental calibration. Furthermore, their numerical character does not give direct guidelines for the noise reduction.

In this paper we develop a simple analytical model of a 3D Noncollinear Optical Parametric Amplifier (NOPA). We assume the type-I noncollinear phase matching in a second-order nonlinear crystal pumped with a monochromatic Gaussian beam. As a consequence we are able to calculate the intensity of the parametric fluorescence for any given signal gain, as well as its spatial and spectral distributions. Moreover, we find the optimal seed mode and the pump waist for which the spontaneous fluorescence is minimal.

The results of our approximated model will never be as accurate as a numerical simulations based on tracing the evolution of the quasi-probability distributions [9], but they can be instantly calculated for various configurations of the parametric amplifiers using the Mathematica 6 script we provide online [10] and thus may provide valuable insight in the applications.

Our model is build around a Bloch-Messiah reduction [11] of an optical parametric amplifier operated without pump depletion. It is a theorem which allows us to find a set of orthogonal, characteristic modes (or eigenmodes) of the amplifier and their respective gains. In case of monochromatic pumping the modes

*Electronic address: migdal@fuw.edu.pl

are input and output beam shapes of the signal and the idler fields at any pair of frequencies matching up to the pump. The main statement of the reduction is that if the amplifier is seeded with a beam matching its characteristic input mode, then this beam is amplified by the associated gain factor and assumes the output characteristic shape on the other end of the amplifier. In addition the spontaneous parametric fluorescence is produced in all of the characteristic output modes and the number of photons scattered into each of those modes is equal to the gain of that mode. In particular the immediate conclusion from the reduction is that the optimal signal to parametric noise ratio is obtained when the seed beam has a shape of the fundamental input mode. The output of the amplifier may be spatially filtered to reject as much of the higher other modes as possible. Let us also note that the Bloch-Messiah reduction allows us to transform a 3D amplifier pumped with a focused beam into a set of independent two-mode OPAs well known from textbooks [12, 13].

We seek the reduction for a low-gain parametric amplifier for an arbitrary pair of signal and idler frequencies. The final result can be expressed in a closed form in two special cases: zero walk-off of the pump beam or for total walk-off of the order of beam size. Characteristic modes of the first setting are optical vortices. The latter case corresponds to the typical experimental situation and we find that the characteristic modes are elliptic Hermite-Gaussian beams. We check the validity of the approximations assumed during the derivation by comparing the analytical result to the numerical calculations for a typical range of parameters. Finally we scale the results of the reduction to the high gain regime using the results of our previous work [14] and we discuss how to calculate the gain and fluorescence intensity.

In particular we find the optimal seed beam, which turns out to be elliptic Gaussian and we give approximate expressions for its diameters. We also find an optimal pump beam waist which provides best suppression of high order modes and the spontaneous fluorescence carried by them.

The paper is organized as follows. Section 2 presents general theory of parametric down-conversion, with emphasis on the 3D crystal pumped by a monochromatic wave. We introduce Bloch-Messiah reduction theorem and discuss its general consequences. In Section 3 we derive the characteristic modes and their gains for two particular settings - noncollinear with no walk-off and noncollinear with a significant walk-off. Section 4 summarizes the results of the analytical reduction. In Section 5 we compare analytical results with precise numerical calculations and discuss the accuracy of the approximations assumed. Section 6 describes behavior of the parametric gain in the intense pumping regime, provides estimation of the fluorescence noise in practical situations and gives solutions for the noise reduction. Finally, Section 7 concludes the paper and gives insight in the possible applications and extensions.

2. BLOCH-MESSIAH REDUCTION

We aim at investigating properties of a 3D parametric amplifier pumped by a strong, monochromatic laser beam of frequency ω_p and diameter $2w_p$. We assume that the signal and the spontaneous fluorescence fields are always so weak that they cannot influence the evolution of the pump. Within this approximation the nonlinear interaction with the pump field couples pairs of conjugate frequencies, commonly called signal ω_s and idler $\omega_i = \omega_p - \omega_s$. Let us note that any two adjacent frequencies $\omega_s \neq \omega'_s$ evolve completely independently thanks to a narrowband pumping. Therefore an amplification of a broadband seed pulse can be calculated separately for each of its monochromatic components which may enter the crystal at different angles [15]. In the following we will analyze an interaction of a particular pair of frequencies ω_s and ω_i with the pump.

We choose a coordinate system where z axis lies along the central k -vector of the pump k_p and the crystal faces are perpendicular to this axis. Then it is most convenient to follow the convention of describing the evolution of the system as a function of z . We expand the electric field of each of the interacting waves in the basis of monochromatic plane waves parameterized by frequency ω and perpendicular components of the wave vector k_x and k_y

$$E(t, x, y, z) = i \int d\omega dk_x dk_y \sqrt{\frac{\hbar\omega}{4\pi\epsilon_0 c \sqrt{n(\omega)}}} e^{-i\omega t + ixk_x + iyk_y} A(\omega, k_x, k_y, z) + \text{c.c.}, \quad (1)$$

where $A(\omega, k_x, k_y, z)$ is z -dependent frequency-space amplitude of the wave. With the above normalization $|A(\omega, k_x, k_y, z)|^2$ is the photon density.

2.1. 1-D amplifier

Before analyzing a bulk amplifier let us briefly recall the basic concepts on a waveguide amplifier which can be reduced into a 2-mode amplifier for a defined signal frequency. This simple system will help in comprehension of the full-fledged 3-D amplifier. Later on the Bloch-Messiah decomposition will allow us to simplify the 3-D amplifier to a set of independent 2-mode amplifiers.

The pump field undergoes only dispersive evolution and its amplitude along the z axis is $A_p(z) = Pe^{ik_{p,z}z}$, where $k_{p,z}$ is the pump wavenumber and P is the initial amplitude. The evolution of the signal amplitude $A_s(z)$ and the idler amplitude $A_i(z)$ are described by equations of motion [16]

$$\begin{aligned}\frac{\partial}{\partial z}A_s(z) &= ik_{s,z}A_s(z) + \chi Pe^{ik_{p,z}z}A_i^*(z) \\ \frac{\partial}{\partial z}A_i(z) &= ik_{i,z}A_i(z) + \chi Pe^{ik_{p,z}z}A_s^*(z).\end{aligned}\quad (2)$$

The wave vectors for the signal and the idler are $k_{s,z}$ and $k_{i,z}$, respectively. The first term on the right hand side is responsible for the linear propagation. The second describes the nonlinear interaction with a coupling constant χ . For a waveguide which starts at $-L/2$ and ends at $L/2$ one can obtain the following input-output relations:

$$\begin{aligned}(e^{i\delta_3}A_s^{out}) &= \cosh(\xi)(e^{i\delta_1}A_s^{in}) + \sinh(\xi)(e^{i\delta_2}A_i^{in})^* \\ (e^{i\delta_4}A_i^{out}) &= \cosh(\xi)(e^{i\delta_2}A_i^{in}) + \sinh(\xi)(e^{i\delta_1}A_s^{in})^*.\end{aligned}\quad (3)$$

Upper indices *in* and *out* denote positions $z = -L/2$ and $z = L/2$, respectively. Phase terms with δ_1 , δ_2 , δ_3 and δ_4 depend on the wave vector matching and we skip their explicit form for brevity. The intensity gain of the amplifier equals $\cosh^2 \xi$, where the gain parameter ξ is proportional to the pump amplitude P . In addition to the amplified signal the interaction produces spontaneous fluorescence. Quantum-mechanical considerations [12] show that the average number of photons generated this way equals $\sinh^2 \xi$. This system is called a 2-mode or nondegenerate parametric amplifier [13]. If one needs to calculate amplification of a realistic laser pulse, the pulse has to be decomposed into monochromatic waves via Fourier transform, amplified as in (3) and composed back.

2.2. Bulk amplifier

Let us now switch to a bulk crystal with length L in the z direction and infinite in the x and y directions. The pump $A_p(\vec{k}_{p,\perp})$, the signal $A_s(\vec{k}_{s,\perp})$ and the idler $A_i(\vec{k}_{i,\perp})$ amplitudes have spatial freedom which is encoded in their dependence on the spatial wave vector $\vec{k}_\perp = (k_x, k_y)$. The infinite transversal size of the crystal allows interaction only of those signal and idler components for which transversal wave vectors sum up to the pump's. Therefore in each slice of the crystal with given z only those interactions can take place, which preserve both the energy $\omega_p = \omega_s + \omega_i$ and the perpendicular components of the momentum

$$\vec{k}_{p,\perp} = \vec{k}_{s,\perp} + \vec{k}_{i,\perp}.\quad (4)$$

Using those principles an equation of motion for the waveguide amplifier (2) can be extended as follows

$$\begin{aligned}\frac{\partial}{\partial z}A_s(\vec{k}_{s,\perp}, z) &= ik_{s,z}A_s(\vec{k}_{s,\perp}, z) + \chi \int d\vec{k}_{i,\perp} A_p(\vec{k}_{s,\perp} + \vec{k}_{i,\perp}) e^{ik_{p,z}z} A_i^*(\vec{k}_{i,\perp}, z) \\ \frac{\partial}{\partial z}A_i(\vec{k}_{i,\perp}, z) &= ik_{i,z}A_i(\vec{k}_{i,\perp}, z) + \chi \int d\vec{k}_{s,\perp} A_p(\vec{k}_{s,\perp} + \vec{k}_{i,\perp}) e^{ik_{p,z}z} A_s^*(\vec{k}_{s,\perp}, z).\end{aligned}\quad (5)$$

As in the waveguide (2), the first term on the right hand side represent the dispersive propagation. The second term is responsible for nonlinear interactions involving all possible planewave components fulfilling (4). The above equations are linear in the signal and the idler amplitudes and so do the input-output relations for the amplifier. Formally they can be written down using input-output relations with integral kernels (or Green functions) $C_{ss}(\vec{k}_{s,\perp}, \vec{k}_{s,\perp})$, $S_{si}(\vec{k}_{s,\perp}, \vec{k}_{i,\perp})$, $C_{ii}(\vec{k}_{i,\perp}, \vec{k}_{i,\perp})$, $S_{is}(\vec{k}_{i,\perp}, \vec{k}_{s,\perp})$

$$\begin{aligned} A_s^{out}(\vec{k}_{s,\perp}) &= \int d\vec{k}'_{s,\perp} C_{ss}(\vec{k}_{s,\perp}, \vec{k}'_{s,\perp}) A_s^{in}(\vec{k}'_{s,\perp}) + \int d\vec{k}_{i,\perp} S_{si}(\vec{k}_{s,\perp}, \vec{k}_{i,\perp}) A_i^{in*}(\vec{k}_{i,\perp}) \\ A_i^{out}(\vec{k}_{i,\perp}) &= \int d\vec{k}'_{i,\perp} C_{ii}(\vec{k}_{i,\perp}, \vec{k}'_{i,\perp}) A_i^{in}(\vec{k}'_{i,\perp}) + \int d\vec{k}_{s,\perp} S_{is}(\vec{k}_{i,\perp}, \vec{k}_{s,\perp}) A_s^{in*}(\vec{k}_{s,\perp}). \end{aligned} \quad (6)$$

Since the integral kernels describe a reversible process, they turn out to be interdependent. The Bloch-Messiah theorem [11] relates their singular value decompositions (SVD): they have common modes and gain parameters, that is

$$\begin{aligned} C_{ss}(\vec{k}_{s,\perp}, \vec{k}'_{s,\perp}) &= \sum_{n=0}^{\infty} \psi_n^{out}(\vec{k}_{s,\perp}) \cosh(\xi_n) \psi_n^{in*}(\vec{k}'_{s,\perp}), & C_{ii}(\vec{k}_{i,\perp}, \vec{k}'_{i,\perp}) &= \sum_{n=0}^{\infty} \phi_n^{out}(\vec{k}_{i,\perp}) \cosh(\xi_n) \phi_n^{in*}(\vec{k}'_{i,\perp}), \\ S_{si}(\vec{k}_{s,\perp}, \vec{k}_{i,\perp}) &= \sum_{n=0}^{\infty} \psi_n^{out}(\vec{k}_{s,\perp}) \sinh(\xi_n) \phi_n^{in}(\vec{k}_{i,\perp}), & S_{is}(\vec{k}_{i,\perp}, \vec{k}_{s,\perp}) &= \sum_{n=0}^{\infty} \phi_n^{out}(\vec{k}_{i,\perp}) \sinh(\xi_n) \psi_n^{in}(\vec{k}_{s,\perp}). \end{aligned} \quad (7)$$

Above $\psi_n^{in}(\vec{k}_{s,\perp})$, $\psi_n^{out}(\vec{k}_{s,\perp})$, $\phi_n^{in}(\vec{k}_{i,\perp})$ and $\phi_n^{out}(\vec{k}_{i,\perp})$ represent the input signal modes, the output signal modes, the input idler modes and the output idler modes respectively while ξ_n are their gain parameters. Mathematically, $\psi_n^{in}(\vec{k}_{s,\perp})$, $\psi_n^{out}(\vec{k}_{s,\perp})$, $\phi_n^{in}(\vec{k}_{i,\perp})$ and $\phi_n^{out}(\vec{k}_{i,\perp})$ are four different sets of orthonormal functions. Physically, they represent characteristic beam shapes in the far field. Modes with different index n do not couple. More precisely, the input-output relations given by (6) can be brought into canonical Bloch-Messiah form if we decompose the signal and the idler amplitudes in the bases of their characteristic modes

$$\begin{aligned} A_s^{in}(\vec{k}_{s,\perp}) &= \sum_{n=0}^{\infty} A_{s,n}^{in} \psi_n^{in}(\vec{k}_{s,\perp}), & A_s^{out}(\vec{k}_{s,\perp}) &= \sum_{n=0}^{\infty} A_{s,n}^{out} \psi_n^{out}(\vec{k}_{s,\perp}), \\ A_i^{in}(\vec{k}_{i,\perp}) &= \sum_{n=0}^{\infty} A_{i,n}^{in} \phi_n^{in}(\vec{k}_{i,\perp}), & A_i^{out}(\vec{k}_{i,\perp}) &= \sum_{n=0}^{\infty} A_{i,n}^{out} \phi_n^{out}(\vec{k}_{i,\perp}). \end{aligned} \quad (8)$$

Substituting the above into (6) and using (7) we find that the whole OPA can be decomposed into set of independent 2-mode amplifiers

$$\begin{aligned} A_{s,n}^{out} &= \cosh(\xi_n) A_{s,n}^{in} + \sinh(\xi_n) A_{i,n}^{in*} \\ A_{i,n}^{out} &= \cosh(\xi_n) A_{i,n}^{in} + \sinh(\xi_n) A_{s,n}^{in*} \end{aligned} \quad (9)$$

where n indexes subsequent independent modes, conventionally sorted by their gains. Note that the above equations have the same form as the input-output relation for the waveguide 2-mode amplifier given in (3). Similarly, intensity gain of the n -th mode equals $\cosh^2 \xi_n$ and the average number of the photons spontaneously scattered into that mode equals $\sinh^2 \xi_n$. Therefore we are interested in finding the characteristic beam shapes $\psi_n^{in}(\vec{k}_{s,\perp})$, $\psi_n^{out}(\vec{k}_{s,\perp})$ and gain parameters ξ_n as this will provide the complete information. In particular seeding the amplifier with its fundamental mode $\psi_0^{in}(\vec{k}_{s,\perp})$ would give us an advantage of obtaining maximal possible gain $\cosh^2 \xi_0$.

Let us make a nontrivial observation. For a special case of the crystal surfaces equally separated from the $z = 0$ plane and with the real pump amplitude in $z = 0$, we get a symmetry $S_{si}(\vec{k}_{s,\perp}, \vec{k}_{i,\perp}) = S_{is}^*(\vec{k}_{i,\perp}, \vec{k}_{s,\perp})$ [14]. When every gain parameter is unique $\xi_n \neq \xi_m$, the input and output signal modes are mirror reflections of each other, as well as the input and output idler modes

$$\psi_n^{out}(\vec{k}_{s,\perp}) = \psi_n^{in*}(\vec{k}_{s,\perp}), \quad \phi_n^{out}(\vec{k}_{i,\perp}) = \phi_n^{in*}(\vec{k}_{i,\perp}). \quad (10)$$

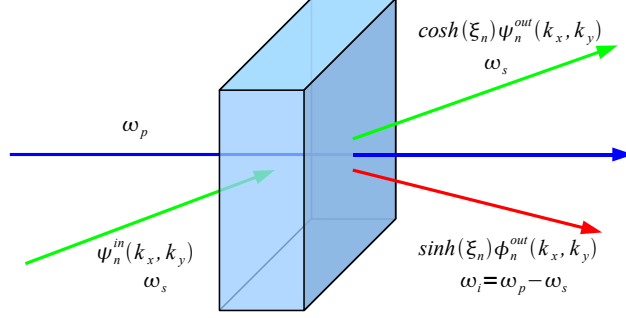


FIG. 1: A schematic of a NOPA pumped with focused monochromatic beam. When an incident signal beam is in the $\psi_n^{in}(\vec{k}_{s,\perp})$ mode, it produces the signal $\psi_n^{out}(\vec{k}_{s,\perp})$ on output with the amplitude amplification of $\cosh(\xi_n)$ and the idler $\phi_n^{out}(\vec{k}_{i,\perp})$ with the amplitude $\sinh(\xi_n)$.

This observation significantly simplifies the Bloch-Messiah reduction given in (7). In particular it allows us to deduce all the characteristic mode functions from the SVD of $S_{is}(\vec{k}_{i,\perp}, \vec{k}_{s,\perp})$.

Even though in and out modes are similar (10), the behavior inside the crystal may be complex. Our description says nothing about what happens between the surfaces - we have only the input-output relations. The shape of the modes, as well as their amplification, vary with a number of parameters, including the crystal length L .

2.3. Perturbative expansion

In general the integral kernels defined in (6) cannot be found analytically. However, one can obtain closed form expressions in a low gain regime $\chi \rightarrow 0$. This is accomplished in two steps. First we assume zero nonlinearity $\chi = 0$. Then the (5) can be immediately integrated as follows

$$A_s(\vec{k}_{s,\perp}, z) = A_s(\vec{k}_{s,\perp}, z=0) \exp[ik_{s,z}(\vec{k}_{s,\perp})z], \quad A_i(\vec{k}_{i,\perp}, z) = A_i(\vec{k}_{i,\perp}, z=0) \exp[ik_{i,z}(\vec{k}_{i,\perp})z], \quad (11)$$

which describes the linear propagation. To obtain the first order approximation with respect to χ , we need to integrate (5) over $-L/2 < z < L/2$ with zeroth-order approximation (11) substituted on the right hand side. Comparing the result to the definition of the integral kernels (6), we obtain

$$C_{ss}(\vec{k}_{s,\perp}, \vec{k}_{s,\perp}) = \exp(ik_{s,z}z) \delta(k'_{s,z} - k_{s,z}), \quad C_{ii}(\vec{k}_{i,\perp}, \vec{k}_{i,\perp}) = \exp(ik_{i,z}z) \delta(k'_{i,z} - k_{i,z}). \quad (12)$$

In the first-order approximation the above functions describe only linear propagation. However, the remaining two kernels

$$\begin{aligned} S_{si}(\vec{k}_{s,\perp}, \vec{k}_{i,\perp}) &= \chi L e^{-i(k_{i,z} - k_{s,z})L/2} A_p(\vec{k}_{i,\perp} + \vec{k}_{s,\perp}) \text{sinc}(\Delta k L/2) \\ S_{is}(\vec{k}_{i,\perp}, \vec{k}_{s,\perp}) &= \chi L e^{i(k_{i,z} - k_{s,z})L/2} A_p(\vec{k}_{i,\perp} + \vec{k}_{s,\perp}) \text{sinc}(\Delta k L/2), \end{aligned} \quad (13)$$

describe down-conversion and give us insight into the characteristic modes of the Bloch-Messiah reduction (7). We call S_{is} the scattering kernel, as it describes amplitudes with which the incident signal creates the 'scattered' idler beam. The Δk is the wave vector mismatch along the z axis in this process

$$\Delta k = k_{s,z} + k_{i,z} - k_{p,z}. \quad (14)$$

The z components of the wave vectors are functions of their transversal wave vector $k_{s,z} = k_{s,z}(\vec{k}_{s,\perp})$, $k_{i,z} = k_{i,z}(\vec{k}_{i,\perp})$ and $k_{p,z} = k_{p,z}(\vec{k}_{i,\perp} + \vec{k}_{s,\perp})$.

Once we perform SVD of the scattering kernel S_{is} (13) we find all characteristic modes and gain parameters of the Bloch-Messiah reduction (7) with help of the identity (10). Obtaining an approximate analytical SVD of the scattering kernel S_{is} is described in the next section. It requires several nontrivial steps. However we will always separate the variables in cylindrical coordinates as follows

$$\begin{aligned}
 S_{is}(k_{i,\perp}, \varphi_i; k_{s,\perp}, \varphi_s) &= K(k_{i,\perp}, k_{s,\perp}) \Phi(\varphi_i, \varphi_s) \\
 &= \left[\sum_n \phi_n^{K,out}(k_{i,\perp}) \cdot \xi_n^K \cdot \psi_n^{K,in}(k_{s,\perp}) \right] \left[\sum_m \phi_m^{\Phi,out}(\varphi_i) \cdot \xi_m^\Phi \cdot \psi_m^{\Phi,in}(\varphi_s) \right] \\
 &= \sum_n \sum_m \underbrace{[\phi_n^{K,out}(k_{i,\perp}) \phi_m^{\Phi,out}(\varphi_i)]}_{\phi_{n,m}^{out}(k_{i,\perp}, \varphi_i)} \underbrace{\xi_n^K \xi_m^\Phi}_{\xi_{n,m}} \underbrace{[\psi_n^{K,in}(k_{s,\perp}) \psi_m^{\Phi,in}(\varphi_s)]}_{\psi_{n,m}^{out}(k_{s,\perp}, \varphi_s)}. \quad (15)
 \end{aligned}$$

Above we express the SVD of S_{is} as a product of SVDs of its radial and angular parts, $K(k_{i,\perp}, k_{s,\perp})$ and $\Phi(\varphi_i, \varphi_s)$. Note that this is also an approximation which relies on the fact that the radial mode functions $\phi_n^{K,out}(k_{i,\perp})$ and $\psi_n^{K,in}(k_{s,\perp})$ are centered around certain $k_\perp \simeq k_0$ and do not extend towards the origin $k_\perp \simeq 0$.

3. ANALYTICAL APPROXIMATION

Our task is to find the SVD of the scattering kernel $S_{is}(\vec{k}_{i,\perp}, \vec{k}_{s,\perp})$ given in (13) for a Gaussian pump beam. We will accurately find a mode with the highest amplification. To obtain the result we go through several approximations as illustrated in Fig. 2. They include replacing sinc with a Gaussian, Taylor expansion of the phase mismatch $\Delta k L/2$ and the separation of variables. We will consider two different physical settings - noncollinear without pump walk-off and noncollinear with a significant pump walk-off. For each of them we obtain closed form Bloch-Messiah reduction, as summarized in Sec. 4. We restrict ourselves to the type I down-conversion, although we conjecture that similar approach may work also for the type II process.

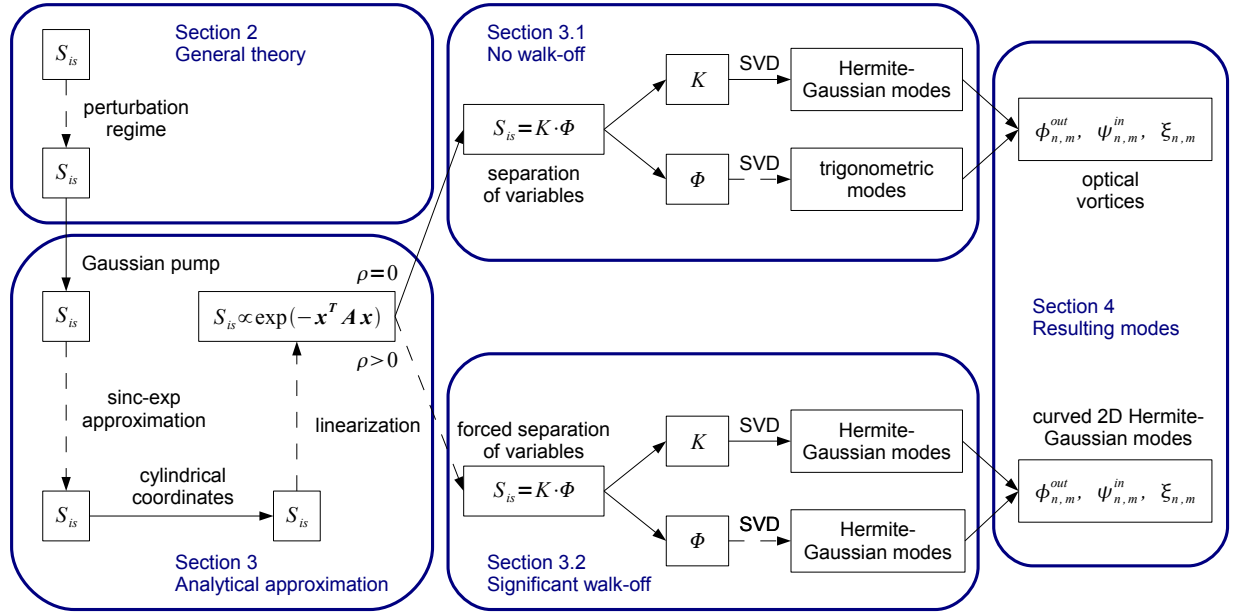


FIG. 2: The scheme of the procedures applied in the Section 3 along with parts of the Section 2 and the Section 4. Solid lines stands for equalities, while dashed lines for approximations. Final results are summarized and discussed in the Section 4.

We choose Gaussian pump beam profile with waist w_p and the wavefront parallel to the crystal surface. The pump amplitude in spatial frequency domain is

$$A_p(k_{p,x}, k_{p,y}) = P \frac{w_p}{\sqrt{\pi}} \exp \left[-\frac{w_p^2}{2} (k_{p,x}^2 + k_{p,y}^2) \right]. \quad (16)$$

where P is an amplitude factor.

In the first step we approximate $\text{sinc}(\Delta k/L)$ with a Gaussian. This erases the oscillating tails but enables further calculations [17]. We write

$$\text{sinc} \left(\frac{\Delta k L}{2} \right) \approx \exp \left[-\frac{(\Delta k L)^2}{20} \right], \quad (17)$$

bearing in mind we chose arbitrarily the width Gaussian fit as illustrated in Fig. 3. Note that the length of the crystal L appears only in the argument of sinc in (13). Consequently, the uncertainty in the numerical factor in the above approximation can be understood as a $\approx 10\%$ uncertainty of the crystal length L .

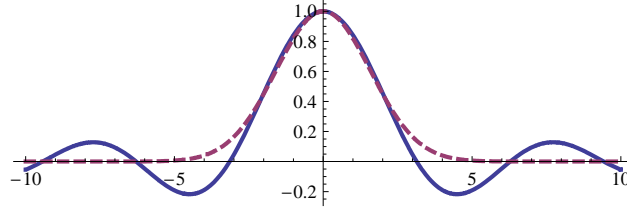


FIG. 3: A plot of $\text{sinc}(x)$ (solid line) and $\exp(-x^2/5)$ (dashed line). In the approximation of sinc with $\exp(-x^2/\kappa)$, reasonable values of the Gaussian width coefficient κ spread from 4.16 to 6.28. One may use the closest Gaussian in the norm distance ($\kappa = 4.16$), set the same FWHM ($\kappa = 5.18$), compare Taylor series up to the second order ($\kappa = 6$) or guarantee the same volume ($\kappa = 6.28$). In various papers [9, 14, 17, 18, 19] different κ were used. We arbitrary set $\kappa = 5$.

Further steps involve Gaussian approximation of the scattering kernel. The task is simple but not straightforward. We need to choose the suitable variables as well as the right Taylor series approximation.

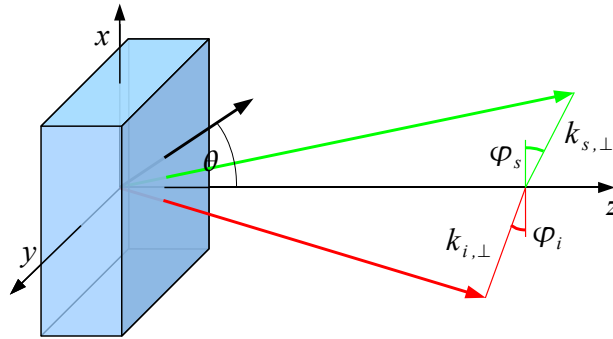


FIG. 4: The crystal in a coordinate system. In both x and y direction the crystal is infinite, while in z its length is L . The optical axis lies in the xz plane, at the angle θ to the z axis.

Since the amplifier discussed has nearly cylindrical symmetry, it is convenient to introduce cylindrical coordinates in the following form

$$\vec{k}_{s,\perp} = [k_{s,\perp} \cos(\varphi_s), k_{s,\perp} \sin(\varphi_s)] \quad \vec{k}_{i,\perp} = [-k_{i,\perp} \cos(\varphi_i), -k_{i,\perp} \sin(\varphi_i)]. \quad (18)$$

Note that angles on the parametric down-conversion cone φ_s and φ_i are measured from 0° and 180° , respectively (Fig. 4). Then the phase matching is achieved for $\varphi_s \approx \varphi_i$. In cylindrical coordinates with approximation (17) the scattering kernel (13) reads

$$S_{is}(k_{i,\perp}, \varphi_i; k_{s,\perp}, \varphi_s) = \chi PL \frac{w_p}{\sqrt{\pi}} e^{i(k_{i,z} - k_{s,z})L/2} \exp \left[-\frac{k_{s,\perp}^2 + k_{i,\perp}^2 - 2k_{s,\perp}k_{i,\perp} \cos(\varphi_s - \varphi_i)}{2/w_p^2} - \frac{1}{20} \Delta k^2 L^2 \right]. \quad (19)$$

The scattering kernel achieves its maximal absolute value when $\vec{k}_{s,\perp} + \vec{k}_{i,\perp} = 0$ and there is no mismatch $\Delta k = 0$. We will linearize Δk around this point, which physically corresponds to the cone of the ideal phase matching.

To calculate the phase mismatch Δk given in (14) we need expressions for the z components of the wave vectors of the interacting waves. We consider type I down-conversion with the signal and the idler propagating as ordinary waves and the pump as extraordinary. We find that

$$\begin{aligned} k_{s,z} &= \sqrt{\frac{\omega_s^2 n_o^2(\omega_s)}{c^2} - k_{s,\perp}^2} \\ k_{i,z} &= \sqrt{\frac{(\omega_p - \omega_s)^2 n_o^2(\omega_p - \omega_s)}{c^2} - k_{i,\perp}^2} \\ k_{p,z} &= (k_{s,x} + k_{i,x}) \frac{\sin(2\theta) [n_o^2(\omega_p) - n_e^2(\omega_p)]}{2 [n_o^2(\omega_p) \sin^2(\theta) + n_e^2(\omega_p) \cos^2(\theta)]} + \frac{n_o(\omega_p) n_e(\omega_p)}{n_o^2(\omega_p) \sin^2(\theta) + n_e^2(\omega_p) \cos^2(\theta)} \\ &\quad \times \sqrt{\left[\frac{\omega^2}{c^2} - \frac{(k_{s,y} + k_{i,y})^2}{n_o^2(\omega_p)} \right] [n_o^2(\omega_p) \sin^2(\theta) + n_e^2(\omega_p) \cos^2(\theta)] - (k_{s,x} + k_{i,x})^2}. \end{aligned} \quad (20)$$

The lengths of the wave vectors of the interacting waves are $k_{s,0}$, $k_{i,0}$ and $k_{p,0}$ and ρ is the tangent of the pump walk-off as illustrated in Fig. 5

$$\begin{aligned} k_{s,0} &= \frac{\omega_s}{c} n_o(\omega_s) & k_{i,0} &= \frac{\omega_p - \omega_s}{c} n_o(\omega_p - \omega_s) \\ k_{p,0} &= \frac{\omega_p}{c} \frac{n_o(\omega_p) n_e(\omega_p)}{\sqrt{n_o^2(\omega_p) \sin^2(\theta) + n_e^2(\omega_p) \cos^2(\theta)}} & \rho &= \frac{\sin(2\theta) [n_o^2(\omega_p) - n_e^2(\omega_p)]}{2 [n_o^2(\omega_p) \sin^2(\theta) + n_e^2(\omega_p) \cos^2(\theta)]}. \end{aligned} \quad (21)$$

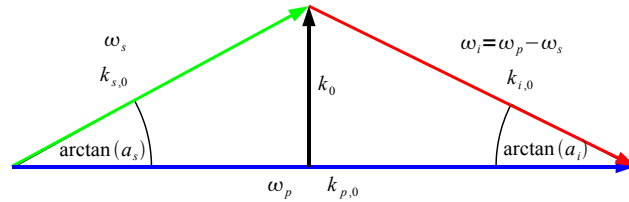


FIG. 5: Scheme of the ideal phase matching. The signal and the idler interacts with the pump central component. Their respective wavenumbers are $k_{s,0}$, $k_{i,0}$ and $k_{p,0}$. The perpendicular wave vector component of both the signal and the idler is k_0 . Inside the crystal, the signal travels at the angle $\arctan(a_s) \approx a_s$ and the idler at $\arctan(a_i) \approx a_i$.

The phase mismatch vanishes $\Delta k = 0$ when $\varphi_s = \varphi_i$ and the perpendicular wave vectors components of the signal and the idler are equal $k_{s,\perp} = k_{i,\perp} = k_0$ with

$$k_0 = \frac{1}{2k_{p,0}} \sqrt{2(k_{s,0}^2 k_{i,0}^2 + k_{p,0}^2 k_{s,0}^2 + k_{p,0}^2 k_{i,0}^2) - k_{s,0}^4 - k_{i,0}^4 - k_{p,0}^4}. \quad (22)$$

The linearization of the Δk given in (14) around its zero with respect to $k_{s,\perp}$, $k_{i,\perp}$ and $(\varphi_s - \varphi_i)$ using (20) gives us

$$\Delta k \approx [a_s - \rho \cos(\frac{\varphi_s + \varphi_i}{2})] (k_{s,\perp} - k_0) + [a_i + \rho \cos(\frac{\varphi_s + \varphi_i}{2})] (k_{i,\perp} - k_0) - k_0 \rho \sin(\frac{\varphi_s + \varphi_i}{2}) (\varphi_s - \varphi_i). \quad (23)$$

Both $a_s = k_0 / \sqrt{k_{s,0}^2 - k_0^2}$ and $a_i = k_0 / \sqrt{k_{i,0}^2 - k_0^2}$ have an easy interpretation. Each of them is a tangent of the angle at which the signal or the idler travels inside the crystal in the ideal phase matching setting. Since ρ (21) is the tangent of the pump walk-off angle, sum and difference of a_s or a_i and ρ reflects how the signal or the idler diverges from the pump.

The Gaussian pump (16) may be approximated by Gaussian function also in cylindrical coordinates (18). For the exponent we obtain

$$k_{s,\perp}^2 + k_{i,\perp}^2 - 2k_{s,\perp}k_{i,\perp} \cos(\varphi_s - \varphi_i) \approx k_0^2(\varphi_s - \varphi_i)^2 + (k_{s,\perp} - k_{i,\perp})^2, \quad (24)$$

which is valid as long as $1/w_p \ll k_0$, that is the down-conversion cone opening angle is much bigger than the pump beam divergence.

Consequently, the scattering kernel S_{is} given in (19) substituted with (23) and (24) becomes a Gaussian function in $k_{s,\perp}$, $k_{i,\perp}$ and $(\varphi_s - \varphi_i)$, that is

$$S_{is}(k_{i,\perp}, \varphi_i; k_{s,\perp}, \varphi_s) = \chi PL \frac{w_p}{\sqrt{\pi}} e^{i(k_{i,z} - k_{s,z})L/2} \exp(-\mathbf{x}^T \mathbf{A} \mathbf{x}), \quad (25)$$

where $\mathbf{x} = [(\varphi_s - \varphi_i), (k_{s,\perp} - k_0), (k_{i,\perp} - k_0)]$ is the deviation from the ideal phase matching. The quadratic form coefficients are

$$\begin{aligned} \mathbf{A} = \begin{bmatrix} A_{\varphi\varphi} & A_{\varphi s} & A_{\varphi i} \\ A_{s\varphi} & A_{ss} & A_{si} \\ A_{i\varphi} & A_{is} & A_{ii} \end{bmatrix} &= \underbrace{\begin{bmatrix} \frac{k_0^2 w_p^2}{2} + \frac{L^2}{20} k_0^2 \rho^2 \sin^2(\frac{\varphi_s + \varphi_i}{2}) & 0 & 0 \\ 0 & 0 & 0 \\ 0 & 0 & 0 \end{bmatrix}}_{\text{the angular part}} \\ &+ \underbrace{\begin{bmatrix} 0 & 0 & 0 \\ 0 & \frac{w_p^2}{2} + \frac{L^2}{20} [a_s - \rho \cos(\frac{\varphi_s + \varphi_i}{2})]^2 & -\frac{w_p^2}{2} + \frac{L^2}{20} [a_s - \rho \cos(\frac{\varphi_s + \varphi_i}{2})] [a_i + \rho \cos(\frac{\varphi_s + \varphi_i}{2})] \\ 0 & -\frac{w_p^2}{2} + \frac{L^2}{20} [a_s - \rho \cos(\frac{\varphi_s + \varphi_i}{2})] [a_i + \rho \cos(\frac{\varphi_s + \varphi_i}{2})] & \frac{w_p^2}{2} + \frac{L^2}{20} [a_i + \rho \cos(\frac{\varphi_s + \varphi_i}{2})]^2 \end{bmatrix}}_{\text{the radial part}} \\ &+ \underbrace{\frac{L^2}{20} k_0 \rho \sin(\frac{\varphi_s + \varphi_i}{2}) \begin{bmatrix} 0 & -[a_s - \rho \cos(\frac{\varphi_s + \varphi_i}{2})] & -[a_i + \rho \cos(\frac{\varphi_s + \varphi_i}{2})] \\ -[a_s - \rho \cos(\frac{\varphi_s + \varphi_i}{2})] & 0 & 0 \\ -[a_i + \rho \cos(\frac{\varphi_s + \varphi_i}{2})] & 0 & 0 \end{bmatrix}}_{\text{the mixed part}} \end{aligned} \quad (26)$$

The matrix \mathbf{A} is presented as sum of different parts to facilitate the separation of variables. We call those components the angular part, the radial part and the mixed part. Once the mixed part is zero, the scattering kernel S_{is} may be written as a product of two kernels, as outlined in (15). We will develop two different approximations: one for no pump walk-off $\rho = 0$ and the other for a significant pump walk-off. The aim of further steps is to neglect the mixed terms and get rid of trigonometric functions.

3.1. No walk-off

In some special situations there may be no walk-off ($\rho = 0$). It is particularly easy to solve, as the quadratic form matrix (25) can be factorized into the angular and the radial part (as the mixed part vanishes)

$$\mathbf{A} = \begin{bmatrix} \frac{k_0^2 w_p^2}{2} & 0 & 0 \\ 0 & \frac{w_p^2}{2} + \frac{L^2}{20} a_s^2 & -\frac{w_p^2}{2} + \frac{L^2}{20} a_s a_i \\ 0 & -\frac{w_p^2}{2} + \frac{L^2}{20} a_s a_i & \frac{w_p^2}{2} + \frac{L^2}{20} a_i^2 \end{bmatrix}. \quad (27)$$

As the scattering kernel may be factorized $S_{is} = K(k_{i,\perp}, k_{s,\perp}) \Phi(\varphi_i, \varphi_s)$ as in (15), we need to find SVDs of two separate parts. To deal with the angular part we write

$$\begin{aligned} \Phi(\varphi_i, \varphi_s) &= \exp \left[-\frac{k_0^2 w_p^2}{2} (\varphi_s - \varphi_i)^2 \right] = \frac{1}{\sqrt{2\pi}} \frac{1}{k_0 w_p} \int_{-\infty}^{\infty} dm \exp \left[-\frac{m^2}{2k_0^2 w_p^2} + im(\varphi_s - \varphi_i) \right] \\ &\approx \frac{1}{\sqrt{2\pi}} \frac{1}{k_0 w_p} \sum_{m=-\infty}^{\infty} \exp(-im\varphi_i) \exp \left(-\frac{m^2}{2k_0^2 w_p^2} \right) \exp(+im\varphi_s). \end{aligned} \quad (28)$$

We applied Fourier representation of a Gaussian function and then we approximated the integration by summation. The second step required moderately slowly changing function, what is guaranteed by $1/w_p \ll k_0$, already required in the previous step (24).

The remaining radial part of the kernel $K(k_{i,\perp}, k_{s,\perp})$ is a quadratic form of $(k_{s,\perp} - k_0)$ and $(k_{i,\perp} - k_0)$. It can be directly decomposed with the Mehler's Hermite polynomial formula [20], which reads

$$\begin{aligned} \exp \left[-\frac{1+\mu^2}{2(1-\mu^2)}(x^2 + y^2) + \frac{2\mu xy}{1-\mu^2} \right] &= \sqrt{\pi} \sqrt{1-\mu^2} \sum_{n=0}^{\infty} \mu^n u_n(x) u_n(y), \\ u_n(x) &= (2^n n!)^{-\frac{1}{2}} H_n(x) \exp(-x^2/2), \end{aligned} \quad (29)$$

where x , y and μ are real numbers, while $u_n(x)$ are the Hermite-Gaussian modes. Comparing coefficient of the radial part $K(k_{i,\perp}, k_{s,\perp})$ found in the lower-right part of (27) with the general Mehler's formula, we get

$$\begin{aligned} K(k_{i,\perp}, k_{s,\perp}) &= \chi PL \frac{w_p}{\sqrt{\pi}} e^{i(k_{i,z} - k_{s,z})L/2} \\ &\times \exp \left[-A_{ss}(k_{s,\perp} - k_0)^2 - 2A_{si}(k_{s,\perp} - k_0)(k_{i,\perp} - k_0) - A_{ii}(k_{i,\perp} - k_0)^2 \right] \\ &= \sum_{n=0}^{\infty} \left\{ e^{ik_{s,z}L/2} \frac{u_n[w_{i,r}(k_{i,\perp} - k_0)]}{\sqrt{1/w_{i,r}}} \right\} \chi PL \frac{w_p}{\sqrt{w_{s,r}w_{i,r}}} \sqrt{1-\mu^2} \mu^n \\ &\times \left\{ e^{-ik_{s,z}L/2} \frac{u_n[w_{s,r}(k_{s,\perp} - k_0)]}{\sqrt{1/w_{s,r}}} \right\} \end{aligned} \quad (30)$$

where μ is a singular value scaling factor while w_s and w_i are width parameters for the signal and the idler, respectively

$$\begin{aligned} |\mu| &= \frac{\sqrt{A_{ss}A_{ii}}}{|A_{si}|} - \sqrt{\frac{A_{ss}A_{ii}}{A_{si}^2} - 1} \\ w_{s,r} &= \sqrt{2A_{ss}} \left(1 - \frac{A_{si}^2}{A_{ss}A_{ii}} \right)^{1/4} \quad w_{i,r} = \sqrt{2A_{ii}} \left(1 - \frac{A_{si}^2}{A_{ss}A_{ii}} \right)^{1/4}. \end{aligned} \quad (31)$$

The coefficients of the quadratic form matrix \mathbf{A} are to be taken from (27). As outlined in (15), once we have SVD of both $K(k_{i,\perp}, k_{s,\perp})$ in (30) and $\Phi(\varphi_i, \varphi_s)$ in (28), we get the resulting S_{is} decomposition for no walk-off $\rho = 0$ case

$$S_{is}(k_{i,\perp}, \varphi_i; k_{s,\perp}, \varphi_s) = \sum_{n=0}^{\infty} \sum_{m=-\infty}^{\infty} \left\{ \frac{e^{ik_{i,z}L/2} u_n[w_{i,r}(k_{i,\perp} - k_0)] \exp(-im\varphi_i)}{\sqrt{1/w_{i,r}}} \frac{\exp(-im\varphi_i)}{\sqrt{2\pi}} \right\} \\ \times \chi PL \frac{\sqrt{2\pi}\sqrt{1-\mu^2}}{k_0\sqrt{w_{s,r}w_{i,r}}} \mu^n \exp\left(-\frac{m^2}{2k_0^2w_p^2}\right) \left\{ \frac{e^{-ik_{s,z}L/2} u_n[w_{s,r}(k_{s,\perp} - k_0)] \exp(im\varphi_s)}{\sqrt{1/w_{s,r}}} \frac{\exp(im\varphi_s)}{\sqrt{2\pi}} \right\}. \quad (32)$$

The resulting modes in no walk-off setting are optical vortices. We discuss this result in Section 4.

3.2. Significant walk-off

The next case of our interest is the setting with a significant walk-off, i.e. when the total walk-off at end of the crystal is order of the pump diameter $L\rho \approx w_p$. Again we take the scattering kernel S_{is} given in (25). The quadratic form \mathbf{A} has nonzero mixed part, which refrains us from the separation of variables. In addition it contains trigonometric functions of the sum of angles $\varphi_s + \varphi_i$.

Let us first consider the physical picture of the significant walk-off setting. An efficient amplification of a beam may be obtained when it travels along the pump. It happens when $\varphi_s + \varphi_i = 0$ or $\varphi_s + \varphi_i = 2\pi$ which corresponds to either signal or idler propagating along the pump. As the distinction between the signal and the idler is illusory, we may assume that the signal is propagating along the pump's walk-off, approximating all expressions containing $\varphi_s + \varphi_i$ around 0. We will hold quadratic term in $A_{\varphi\varphi}$ and only constant term everywhere else in \mathbf{A} . Consequently terms $A_{\varphi s} = A_{s\varphi}$ and $A_{\varphi i} = A_{i\varphi}$ disappear. Thus the quadratic form reads

$$\mathbf{A} = \begin{bmatrix} \frac{k_0^2 w_p^2}{2} + \frac{L^2}{20} k_0^2 \rho^2 \left(\frac{\varphi_s + \varphi_i}{2}\right)^2 & 0 & 0 \\ 0 & \frac{w_p^2}{2} + \frac{L^2}{20} (a_s - \rho)^2 & -\frac{w_p^2}{2} + \frac{L^2}{20} (a_s - \rho)(a_i + \rho) \\ 0 & -\frac{w_p^2}{2} + \frac{L^2}{20} (a_s - \rho)(a_i + \rho) & \frac{w_p^2}{2} + \frac{L^2}{20} (a_i + \rho)^2 \end{bmatrix} \quad (33)$$

Again, we have separated the variables $S_{is} = K(k_{i,\perp}, k_{s,\perp})\Phi(\varphi_i, \varphi_s)$ according to the scheme given in (15). The radial part $K(k_{i,\perp}, k_{s,\perp})$ decomposes with the Mehler's formula (29) as we did for the no-walk-off case. All the coefficients are the same as given in (31), with the quadratic form coefficient matrix \mathbf{A} taken from a significant walk-off approximation matrix (33).

The angular part $\Phi(\varphi_i, \varphi_s)$ contains not only $(\varphi_s + \varphi_i)^2$ but also $(\varphi_s + \varphi_i)^2(\varphi_s - \varphi_i)^2$ terms. They are difficult to handle, so we try the following approximation, with real variables p, q, x, and y

$$\exp[-p^2(1 + q^2 y^2)x^2] \approx \exp(-p^2 x^2 - p^2 q^2 \langle x^2 \rangle y^2) = \exp\left(-p^2 x^2 - \frac{1}{2} q^2 y^2\right). \quad (34)$$

That is, instead of $x^2 y^2$ term we took y^2 times mean x^2 , averaged over the $\exp(-p^2 x^2)$ distribution. The rough approximation (34) is numerically checked to produce the similar characteristic modes and gain parameters as long as $q^2 \ll 1$. In our case $q^2 = L^2 \rho^2 / (40 w_p^2)$ - so the total walk-off cannot be much larger than the pump width $L\rho \ll \sqrt{40} w_p$. With the approximation (34) the angular part $\Phi(\varphi_i, \varphi_s)$ is a quadratic form of φ_s and φ_i . Utilizing once again Mehler's formula (29) we decompose $\Phi(\varphi_i, \varphi_s)$ in the basis of Hermite-Gaussian modes

$$\Phi(\varphi_i, \varphi_s) = \exp\left[-\frac{k_0^2 w_p^2}{2} (\varphi_s - \varphi_i)^2 - \frac{L^2 \rho^2}{20 w_p^2} \left(\frac{\varphi_s + \varphi_i}{2}\right)^2\right] \\ = \sum_{m=0}^{\infty} \left[\frac{u_m(k_0 w_\varphi \varphi_i)}{\sqrt{1/(k_0 w_\varphi)}} \right] \frac{1}{k_0 w_\varphi} \sqrt{\pi} \sqrt{1 - \mu_\varphi^2} \mu_\varphi^m \left[\frac{u_m(k_0 w_\varphi \varphi_s)}{\sqrt{1/(k_0 w_\varphi)}} \right] \quad (35)$$

where μ_φ is the singular value scaling factor while $k_0 w_\varphi$ is the angular width parameter for both the signal and the idler

$$\mu_\varphi = \left(1 - \frac{1}{2\sqrt{10}} \frac{L\rho}{k_0 w_p^2}\right) / \left(1 + \frac{1}{2\sqrt{10}} \frac{L\rho}{k_0 w_p^2}\right) \quad k_0 w_\varphi = \frac{1}{\sqrt[4]{10}} \sqrt{Lk_0\rho}. \quad (36)$$

Hence, we obtain SVD of the scattering kernel S_{is} in the significant walk-off approximation (33) with separated variables (15), which reads

$$S_{is}(k_{i,\perp}, \varphi_i; k_{s,\perp}, \varphi_s) = \sum_{n=0}^{\infty} \sum_{m=0}^{\infty} \left\{ e^{ik_{i,z}L/2} \frac{u_n[w_{i,r}(k_{i,\perp} - k_0)]}{\sqrt{1/w_{i,r}}} \frac{u_m(k_0 w_\varphi \varphi_i)}{\sqrt{1/(k_0 w_\varphi)}} \right\} \\ \times \chi PL \frac{w_p \sqrt{\pi} \sqrt{1-\mu^2} \sqrt{1-\mu_\varphi^2}}{k_0 w_\varphi \sqrt{w_{s,r} w_{i,r}}} \mu^n \mu_\varphi^m \left\{ e^{-ik_{s,z}L/2} \frac{u_n[w_{s,r}(k_{s,\perp} - k_0)]}{\sqrt{1/w_{s,r}}} \frac{u_m(k_0 w_\varphi \varphi_s)}{\sqrt{1/(k_0 w_\varphi)}} \right\}. \quad (37)$$

The further discussion of the modes is in the Section 4.

4. CHARACTERISTIC MODES OF THE AMPLIFIER

In the Section 3 we applied series of approximation to obtain the singular value decomposition of the scattering kernel S_{is} (13). The SVDs for no walk-off (32) and significant walk-off (37) settings were compared with the general Bloch-Messiah reduction (7). We identified the signal $\psi_{n,m}^{out}(k_{s,\perp}, \varphi_s) = \psi_{n,m}^{in*}(k_{s,\perp}, \varphi_s)$ and the idler $\phi_{n,m}^{out}(k_{i,\perp}, \varphi_i) = \phi_{n,m}^{in*}(k_{i,\perp}, \varphi_i)$ modes - see (7) and Fig. 1. In particular the highest achievable amplitude amplification $\xi_{0,0}$ is obtained with the seed $\psi_{0,0}^{in}(k_{s,\perp}, \varphi_s)$ on the input, which produces $\psi_{0,0}^{in*}(k_{s,\perp}, \varphi_s)$ on the output. Let us remind that the amplitudes in the spatial frequency domain are effectively the far-field image.

4.1. No walk-off

In the setting with no walk-off $\rho = 0$ the modes resulting from the solution (32) are optical vortices

$$\psi_{n,m}^{out*}(k_{s,\perp}, -\varphi_s) = \psi_{n,m}^{in}(k_{s,\perp}, \varphi_s) = e^{-ik_{s,z}L/2} \frac{u_n[w_{s,r}(k_{s,\perp} - k_0)]}{\sqrt{1/w_{s,r}}} \frac{\exp(im\varphi_s)}{\sqrt{2\pi}} \\ \phi_{n,m}^{out*}(k_{i,\perp}, -\varphi_i) = \phi_{n,m}^{in}(k_{i,\perp}, \varphi_i) = e^{-ik_{i,z}L/2} \frac{u_n[w_{i,r}(k_{i,\perp} - k_0)]}{\sqrt{1/w_{i,r}}} \frac{\exp(-im\varphi_i)}{\sqrt{2\pi}}. \quad (38)$$

The minus sign at the φ_s and φ_i angles is a nontrivial consequence of twofold degeneracy of the singular values, which changes relations (10). The above modes are trigonometric functions on the down-conversion cone as plotted in Fig. 6. Their shape in the radial direction is that of Hermite-Gaussian function with the width parameter

$$w_{s,r} = \sqrt[4]{1-\nu^{-1}} \sqrt{w_p^2 + \frac{L^2}{10} a_s^2} \quad w_{i,r} = \sqrt[4]{1-\nu^{-1}} \sqrt{w_p^2 + \frac{L^2}{10} a_i^2}, \quad (39)$$

for the signal and the idler respectively, where $\nu = \left(w_p^2 + \frac{L^2}{10} a_s^2\right) \left(w_p^2 + \frac{L^2}{10} a_i^2\right) / \left(-w_p^2 + \frac{L^2}{10} a_s a_i\right)^2$. The gain parameters are

$$\xi_{n,m} = \chi PL \frac{\sqrt{2\pi} \sqrt{1-\mu^2}}{k_0 \sqrt{w_{s,r} w_{i,r}}} \mu^n \exp\left(-\frac{m^2}{2k_0^2 w_p^2}\right), \quad |\mu| = \sqrt{\nu} - \sqrt{\nu-1}. \quad (40)$$

The characteristic modes are optical vortices [21], thanks to the $\exp(im\varphi_s)$ factor. Each of them carry orbital angular momentum, $\hbar m$ per photon. As the spontaneous down-conversion creates entangled photon pairs with the opposite angular momenta [22], they may be used in the field of quantum cryptography [23]. The advantages of using the entangled vortex states as a media for quantum information includes easy measurement [24] and possibility to create Hilbert space of an arbitrary dimension [25].

To obtain the above decomposition we assumed that: $1/w_p \ll k_0$, $1/w_{s,r} \ll k_0$ and $1/w_{i,r} \ll k_0$. This is approximately equivalent to the requirement that beam diffraction angles are much smaller than the angle between signal or idler and the pump.

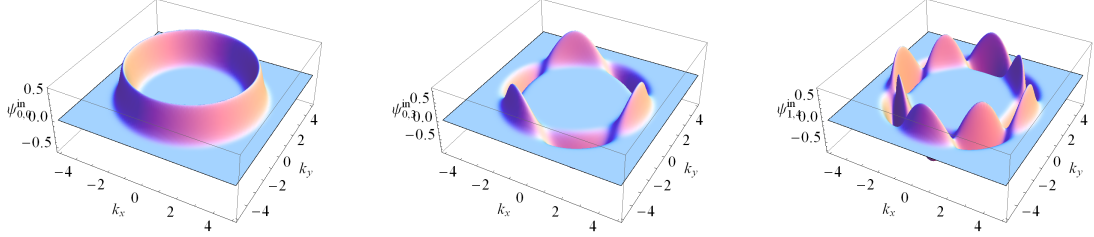


FIG. 6: Three different modes for no walk-off case: $\psi_{0,0}^{in}(k_{s,\perp}, \varphi_s)$, $\psi_{0,3}^{in}(k_{s,\perp}, \varphi_s)$ and $\psi_{1,4}^{in}(k_{s,\perp}, \varphi_s)$. The phase $e^{-ik_{s,z}L/2}$ is not shown. The figure represents the real part of the modes which, due to the degeneracy, are also proper characteristic modes.

4.2. Significant walk-off

In the setting with a significant walk-off $\rho > 0$ the modes resulting from (37) are elliptic Hermite-Gaussian beams

$$\begin{aligned} \psi_{n,m}^{out*}(k_{s,\perp}, \varphi_s) &= \psi_{n,m}^{in}(k_{s,\perp}, \varphi_s) = e^{-ik_{s,z}L/2} \frac{u_n[w_{s,r}(k_{s,\perp} - k_0)]}{\sqrt{1/w_{s,r}}} \frac{u_m(k_0 w_\varphi \varphi_s)}{\sqrt{1/(k_0 w_\varphi)}} \\ \phi_{n,m}^{out*}(k_{i,\perp}, \varphi_i) &= \phi_{n,m}^{in}(k_{i,\perp}, \varphi_i) = e^{-ik_{i,z}L/2} \frac{u_n[w_{i,r}(k_{i,\perp} - k_0)]}{\sqrt{1/w_{i,r}}} \frac{u_m(k_0 w_\varphi \varphi_i)}{\sqrt{1/(k_0 w_\varphi)}}. \end{aligned} \quad (41)$$

as plotted in Fig. 7. That is, the characteristic modes are 2D Hermite-Gaussian functions, curved on the down-conversion cone. Their widths parameters are

$$\begin{aligned} w_{s,r} &= \sqrt[4]{1-\nu^{-1}} \sqrt{w_p^2 + \frac{L^2}{10}(a_s - \rho)^2} & w_{i,r} &= \sqrt[4]{1-\nu^{-1}} \sqrt{w_p^2 + \frac{L^2}{10}(a_i + \rho)^2} \\ k_0 w_\varphi &= \frac{1}{\sqrt[4]{10}} \sqrt{L k_0 \rho} & \nu &= \frac{\left[w_p^2 + \frac{L^2}{10}(a_s - \rho)^2\right] \left[w_p^2 + \frac{L^2}{10}(a_i + \rho)^2\right]}{\left[-w_p^2 + \frac{L^2}{10}(a_s - \rho)(a_i + \rho)\right]^2}. \end{aligned} \quad (42)$$

The respective gain parameters are

$$\xi_{n,m} = \chi PL \frac{w_p \sqrt{\pi} \sqrt{1-\mu^2} \sqrt{1-\mu_\varphi^2}}{k_0 w_\varphi \sqrt{w_{s,r} w_{i,r}}} \mu^n \mu_\varphi^m, \quad |\mu| = \sqrt{\nu} - \sqrt{\nu-1}, \quad \mu_\varphi = \frac{1 - \frac{1}{2\sqrt{10}} \frac{L\rho}{k_0 w_p^2}}{1 + \frac{1}{2\sqrt{10}} \frac{L\rho}{k_0 w_p^2}}. \quad (43)$$

To obtain the above decomposition we assumed that: $1/w_p \ll k_0$, $1/w_{s,r} \ll k_0$, $1/w_{i,r} \ll k_0$, $1/k_0 w_\varphi \ll \pi$ and $L\rho/\sqrt{40} \ll w_p$. In other words, beam diffraction angles need to be much smaller than the phase matching

angles, the total walk-off cannot be much larger than the pump waist and the mode arc width have to be smaller than π .

When the angular width is relatively small, the modes are just elliptic Hermite-Gaussian functions [26] in spatial frequencies. The explicit condition is $w_{s,r} \ll k_0 w_\varphi^2$ for the signal and $w_{i,r} \ll k_0 w_\varphi^2$ for the idler. Then the Fourier transform of (41) gives representation in space in the near field

$$\begin{aligned}\psi_{n,m}^{out*}(-x, -y) &= \psi_{n,m}^{in}(x, y) = e^{-ik_0 x} \frac{u_n\left(\frac{x+a_s L/2}{w_{s,r}}\right)}{\sqrt{w_{s,r}}} \frac{u_m\left(\frac{y}{w_\varphi}\right)}{\sqrt{w_\varphi}} \\ \phi_{n,m}^{out*}(-x, -y) &= \phi_{n,m}^{in}(x, y) = e^{ik_0 x} \frac{u_n\left(\frac{x-a_i L/2}{w_{i,r}}\right)}{\sqrt{w_{i,r}}} \frac{u_m\left(\frac{y}{w_\varphi}\right)}{\sqrt{w_\varphi}}\end{aligned}\quad (44)$$

In particular the $\psi_{0,0}^{in}(x, y)$ is an elliptical Gaussian beam, traveling along the ideal phase matching cone, that is, at the angle $\arctan(a_s)$ and passing through the center of the crystal. Its widths are $w_{s,r}$ in the radial direction and w_φ in the angular direction. The mode is optimal in the terms of maximal achievable gain, as well as the signal-to-noise ratio.

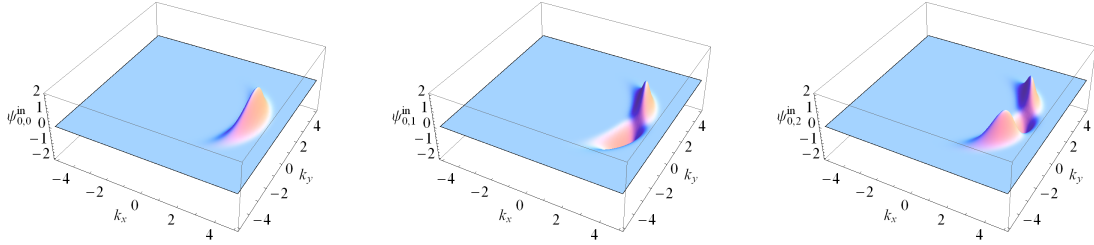


FIG. 7: First three modes for significant walk-off case: $\psi_{0,0}^{in}(k_{s,\perp}, \varphi_s)$, $\psi_{0,1}^{in}(k_{s,\perp}, \varphi_s)$ and $\psi_{0,2}^{in}(k_{s,\perp}, \varphi_s)$. The phase $e^{-ik_{s,z} L/2}$ is not shown. The modes are bent elliptic Gaussian-Hermite beams. When angular width is sufficiently small, the mode with highest amplification $\psi_{0,0}^{in}(k_{s,\perp}, \varphi_s)$ is just elliptic Gaussian.

5. NUMERICAL SIMULATIONS

Above, we have derived the singular value decompositions (32) and (37) from the low gain regime scattering kernel S_{is} given in (13). However, along with mathematically well justified approximations we have taken a few less rigorous steps, especially (17) and (34). Furthermore, separation of variables (15) need to be verified, as well as the Taylor series approximation around the $\varphi_s + \varphi_i = 0$, (33). To confirm the validity of the derivation of the characteristic modes we performed a numerical simulation.

For each crucial step in the approximation of the scattering kernel S_{is} , we performed its numerical SVD. Technically, we calculated a discretized kernel in cylindrical coordinate system (18), corrected with the proper Jacobian. It was too memory consuming to calculate S_{is} over entire rectangular sector of the coordinate grid, so we calculated its values only in regions which have a potential to contribute significantly and we employed sparse arrays. Since S_{is} (13) has the pump amplitude (16) as a factor, we took into account only those regions in $(\vec{k}_{i,\perp}, \vec{k}_{s,\perp})$ space for which values of $A_p(\vec{k}_{s,\perp} + \vec{k}_{i,\perp})$ are significant. In the cylindrical coordinates this happens when

$$|k_{s,\perp} - k_{i,\perp}| < \frac{2.5}{w_p} \quad \text{and} \quad |\varphi_s - \varphi_i| < \frac{2.5}{k_0 w_p}. \quad (45)$$

We chose the constant 2.5 as it covers over 0.999 of the pump intensity. Moreover, we restricted ourselves to values close to the ideal phase matching setting $k_{s,\perp}$, $k_{i,\perp} \simeq k_0$ and φ_s , $\varphi_i \simeq 0$. The extent of the grid

must be much greater than the zeroth mode, while the mesh must be much smaller than the peak sizes. The requirement is especially important for the sinc peak, as too low resolution may spoil its oscillating shape. To check if the simulation works properly, we compared results for the same physical data but plotted over a twice finer grid or at a twice broader range.

After verifying the reliability of numerical SVD, we have compared results from different scattering kernel S_{is} approximations for a significant walk-off setting. The results are illustrated in Fig. 8. For this data the zeroth singular value $\xi_{0,0}$ was preserved by the approximation, within 2% margin of error. However, other gain parameters changed visibly with every approximation. The radial shape of the zeroth mode was altered only by the sinc-exp approximation (17). Even though the consecutive approximations modified the angular width $w_{s,\varphi}$, the modes were still qualitatively Hermite-Gaussians. Ten first characteristic modes were verified to be indeed well separable. They could be reproduced by a product of radial and angular functions in over 98% of their intensity.

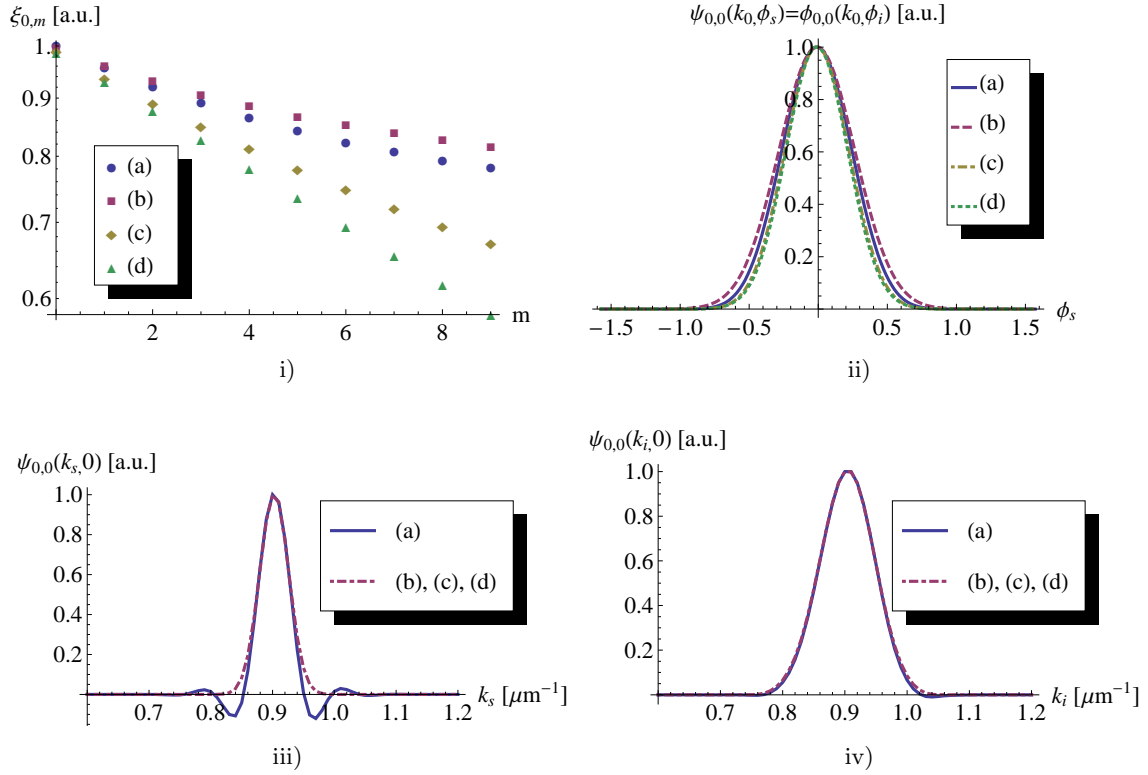


FIG. 8: Comparison of i) the gain parameters $\xi_{0,m}$ and ii-iv) sections through mode functions obtained for four different approximations of the scattering kernel S_{is} : (a) the original with sinc (13), (b) the kernel with exp (19), (b') the quadratic form approximation (25), (c) the kernel with removed the mixed term (33) and (d) the final result (37). As (b) and (b') were indistinguishable, they are represented only by (b). Calculations were carried out for β -BBO crystal with $L = 1\text{mm}$, $\theta = 30^\circ$, $w_p = 20\mu\text{m}$, $\lambda_p = 0.4\mu\text{m}$, $\lambda_s = 0.6\mu\text{m}$. This corresponds to significant walk-off, $\rho L/w_p \approx 2.4$. The kernels have been calculated on a grid of 61×161 points, covering range $[0.6\mu\text{m}^{-1}, 1.2\mu\text{m}^{-1}] \times [-\frac{\pi}{2}, \frac{\pi}{2}]$.

6. PRACTICAL SIGNAL OPTIMIZATION AND NOISE REDUCTION

In the previous chapters we worked in the perturbative regime, that is we assumed that the gain parameters are small $\xi_{n,m} \ll 1$. In particular, we found that the gain parameters are proportional to the pump

amplitude $\xi_{n,m} \propto P$ and the characteristic modes do not change with the pump amplitude P . However, an useful amplifier requires gain parameters much higher than 1. Hence, we need to extrapolate the results. We conjecture that proportionality relation $\xi_{n,m} \propto P$ holds also for higher gains, while the mode functions remain unchanged. This is strictly true for a 1-D parametric amplifier we considered in Sec. 2 and was numerically verified for a waveguide amplifier pumped with ultrashort pulses [14].

In a seeded OPA two processes occur in parallel - amplification of the seed beam and generation of the spontaneous parametric fluorescence. They do not influence one another as long as the saturation effects can be neglected. Both those process can be described within the framework of the developed model. The latter process typically sets the noise level of the amplifier. Since the total amount of fluorescence depends only on the pump parameters and not on the seed, it is best to chose the seed beam size which provides maximum possible amplification. This is exactly the beam described by the fundamental input mode $\psi_{0,0}^{in}(\vec{k}_{s,\perp})$ given in (41) and (44). In a typical situation this is an elliptic Gaussian beam of size $w_{s,r} \times w_\varphi$ propagating at an angle $\arctan(a_s)$ inside the nonlinear crystal. In the interaction with the pump light the seed beam is amplified by a factor $G = \exp(2\xi_{0,0})$ and a beam in a mode $\psi_{0,0}^{out}(\vec{k}_{s,\perp})$ is produced at the output.

If astigmatic shaping of the input beam is unfeasible, one can use round Gaussian beam of the waist $w_s = \sqrt{w_{s,r}w_\varphi}$. In such case many input modes $\psi_{2n,2m}^{in}(\vec{k}_{s,\perp})$ will be excited, each of them will be amplified by a factor $\exp(2\xi_{2n,2m})$ and a distorted beam will be produced on the output. Typically we may neglect higher order modes, since they both have lower gains and are only slightly excited. The most important effect of using round input beam is a reduced coupling of the seed light to the fundamental mode. This is described by the factor

$$\eta = \frac{4w_{s,r}w_{s,\varphi}}{(w_{s,r} + w_{s,\varphi})^2} \quad (46)$$

which effectively reduces gain to ηG .

Let us now proceed to the calculation of the intensity of the fluorescence noise emitted per unit time in a certain direction. From the basic quantum-mechanical considerations we know that the number of photons scattered into mode $\psi_{n,m}^{out}(\vec{k}_{s,\perp})$ at a frequency ω_s is equal to $\sinh^2 \xi_{n,m} \simeq \exp(2\xi_{n,m})$. When we observe the output of the amplifier through an aperture, the contributions of distinct modes should be added incoherently. Thus the spectral density of the number of photons is equal to the sum

$$\langle \tilde{n}(\omega_s) \rangle = \sum_{n,m} \exp(2\xi_{n,m}) T_{n,m} \quad (47)$$

where $T_{n,m}$ is the transmission of the output mode $\psi_{n,m}^{out}(\vec{k}_{s,\perp})$ trough the observation aperture.

To calculate the number of fluorescence photons emitted per unit time $d\langle n \rangle / dt$ we add contributions from all frequencies

$$\frac{d\langle n \rangle}{dt} = \int d\omega_s \langle \tilde{n}(\omega_s) \rangle, \quad (48)$$

where the integral should be performed over the observation bandwidth. With such formulation the pump intensity and the number of fluorescence photons emitted per unit time $d\langle n \rangle / dt$ can become a slowly varying time dependent quantities. Let us however focus on the simplest way of minimizing the total noise represented by the integral (48), that is minimizing the noise power at each frequency $\tilde{n}(\omega_s)$ independently. We consider achieving this goal by spatial filtering of the output of the amplifier with an aperture.

As one may find in (43) the gain parameters $\xi_{n,m}$ form geometric series with respect to both n and m as $\xi_{n,m} \propto \mu^n \mu_\varphi^m$. For a typical data μ is small and modes with $n > 0$ can be neglected. On the contrary μ_φ is often close to 1 and spatial filtering in the angular direction can be necessary. This can be accomplished by imaging the crystal onto suitably oriented slit. One may then achieve high transmission for the fundamental mode $T_{0,0}$ carrying useful signal and significant suppression of higher order mode $T_{0,m}$ as plotted in Fig. 9 or can be checked with a script we provide online [10]. The explicit expression for the intensity transmission

of $\psi_{n,m}^{out}(\vec{k}_{s,\perp})$ mode through the slit of the width h is given by the integral

$$T_{n,m} = \int_{-h/2}^{h/2} dy u_m^2\left(\frac{y}{w_\varphi}\right), \quad (49)$$

where $u_m(y/w_\varphi)$ are the angular components of the mode functions (44).

Another approach to reducing fluorescence contained in high order modes is reducing angular gain decrement μ_φ . Our simplified model predicts that it would approach zero when the following relation holds between the crystal length and the pump beam waist

$$w_p = \frac{1}{\sqrt{2\sqrt{10}}} \sqrt{\frac{L\rho}{k_0}}. \quad (50)$$

Naturally the above relation should be considered approximate, because it relies on the numerical factor used in sinc approximation (17). Fortunately, even a robust fit to the (50) should suffice.

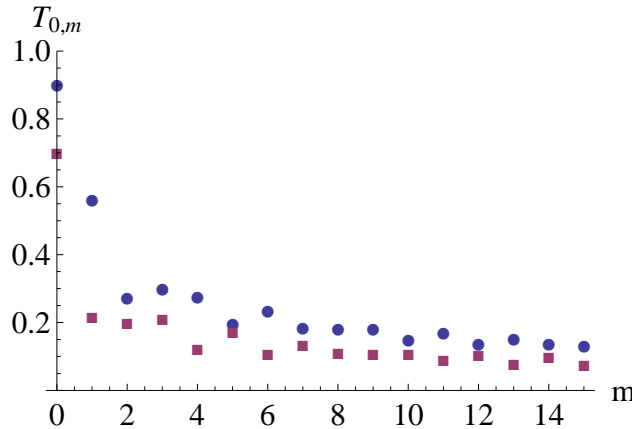


FIG. 9: Plot of the intensity transmittance $T_{0,m}$ of the first 15 Hermite-Gaussian modes through a slit set to transmit 70% (squares) or 90% (dots) of the zeroth mode.

7. CONCLUSION

We have developed simple analytical model of a noncollinear parametric amplifier pumped with a focused monochromatic beam and utilizing type I phase matching. We have found analytically an approximate Bloch-Messiah reduction for settings with and without walk-off. The reduction was obtained in a low gain regime, but we conjecture that it can be scaled to high gain regime using exponential scaling found in prior numerical simulations [14].

In particular we have calculated fundamental mode of the amplifier, which turned out to be elliptic Gaussian. Seeding the amplifier with beam matching this mode yields highest possible amplification. The output of the parametric amplifier contains both amplified seed beam and an optical noise due to parametric fluorescence. The Bloch-Messiah reduction allows us to directly calculate the amount of parametric fluorescence emitted by the amplifier. Further analysis shows that it can be reduced by either suitable spatial filtering of high-order modes or adjusting the pump beam diameter such that those modes are suppressed.

Our results may be also used as a starting point for the numerical code modeling OPCPA with pump depletion. This would be accomplished by dividing the amplifier longitudinally into two parts: the front in which a gain of 10^3 – 10^6 is reached without depleting the pump and the rear where the saturation occurs. The

front part can be treated with our model which gives the seed beam shape and spatially resolved parametric fluorescence intensity. This would be the input to the numerical code solving the classical evolution of the fields in the rear part of the amplifier.

The model developed in this paper may be also helpful for optimizing photon pair sources, since it represents an alternative approach to the problem of finding spatial modes of the parametric fluorescence and optimal fiber coupling [18].

Acknowledgments

We acknowledge insightful discussions with Konrad Banaszek and Czesław Radzewicz, as well as financial support from Polish Government scientific grant (2007-2009).

-
- [1] A. Dubietis, G. Jonušauskas, and A. Piskarskas, Opt. Commun. **88**, 437 (1992).
 - [2] A. Dubietis, R. Butkus, and A. Piskarskas, IEEE J. Sel. Top. Quant. **12**, 163 (2006).
 - [3] I. N. Ross, P. Matousek, G. H. C. New, and K. Osvey, J. Opt. Soc. Am. B **19**, 2945 (2002).
 - [4] F. Tavella, A. Marcinkevicius, and F. Krausz, Opt. Express **14**, 12822 (2006).
 - [5] G. Arisholm, J. Opt. Soc. Am. B **16**, 117 (1999).
 - [6] F. Tavella, K. Schmid, N. Ishii, A. Marcinkevicius, L. Veisz, and F. Krausz, Appl. Phys. B **81**, 753 (2005).
 - [7] F. Tavella, A. Marcinkevicius, and F. Krausz, NJP **8**, 219 (2006).
 - [8] A. Gatti, H. Wiedemann, L. A. Lugiato, I. Marzoli, G.-L. Oppo, and S. M. Barnett, Phys. Rev. A **56**, 877 (1997).
 - [9] J. Chwedenczuk and W. Wasilewski, Phys. Rev. A **78**, 063823 (2008), arXiv:0804.3245v1.
 - [10] URL <http://migdal.wikidot.com/en:downconversion/>.
 - [11] S. L. Braunstein, Phys. Rev. A **71**, 055801 (2005), arXiv:quant-ph/9904002.
 - [12] R. Loudon, *The Quantum Theory of Light* (Oxford University Press, USA, 2000).
 - [13] R. W. Boyd, *Nonlinear optics, Second edition* (Academic press, 2003).
 - [14] W. Wasilewski, A. I. Lvovsky, K. Banaszek, and C. Radzewicz, Phys. Rev. A **73**, 063819 (2006), arxiv:quant-ph/0512215.
 - [15] R. Danielius, A. Piskarskas, P. D. Trapani, A. Andreoni, C. Solcia, and P. Fog, Opt. Lett. **21**, 973 (1996).
 - [16] Y. B. Band, C. Radzewicz, and J. S. Krasinski, Phys. Rev. A **49**, 517 (1994).
 - [17] P. Kolenderski, W. Wasilewski, and K. Banaszek, Phys. Rev. A **80**, 013811 (2009), arXiv:0905.0009.
 - [18] A. Dragan, Phys. Rev. A **70**, 053814 (2004), arXiv:quant-ph/0407113.
 - [19] A.B. Uren, K. Banaszek, and I. Walmsley, arXiv:quant-ph/0305192 (2003).
 - [20] F. A. Barone, H. Boschi-Filho, and C. Farina, Am. J. Phys. **71**, 483 (2003), arXiv:quant-ph/0205085.
 - [21] L. Allen, M. W. Beijersbergen, R. J. C. Spreeuw, and J. P. Woerdman, Phys. Rev. A **45**, 8185 (1992).
 - [22] J. P. Torres, G. Molina-Terriza, and L. Torner, J. Opt. B: Quantum Semiclass. Opt. **7**, 235 (2005).
 - [23] A. Mair, A. Vaziri, G. Weihs, and A. Zeilinger, Nature **412**, 313 (2001).
 - [24] J. Leach, M. J. Padgett, S. M. Barnett, S. Franke-Arnold, and J. Courtial, Phys. Rev. Lett. **88**, 257901 (2002).
 - [25] J. P. Torres, Y. Deyanova, L. Torner, and G. Molina-Terriza, Phys. Rev. A **67**, 052313 (2003).
 - [26] S. P. Walborn, S. Pádua, and C. H. Monken, Phys. Rev. A **71**, 053812 (2005), arXiv:quant-ph/0407216.